Article citation info:
Szwajca F, Skobiej K, Wittek K. Simulation analysis of a gas engine with various prechamber neck diameters in lean burning condition. Rail Vehicles/Pojazdy Szynowe. 2024;1-2:3-10. https://doi.org/10.53502/RAIL-183642

Rail Vehicles/Pojazdy Szynowe

www.railvehicles.eu

Simulation analysis of a gas engine with various prechamber neck diameters in lean burning condition

Filip **Szwajca** [a, *], Kinga **Skobiej** [b], Kamil **Wittek** [b]

[a] *Faculty of Civil and Transport Engineering, Poznan University of Technology, Poland*
[b] *Faculty of Transport and Aviation Engineering, Silesian University of Technology, Poland*

ARTICLE INFO

Received: 21 November 2023
Revised: 23 January 2024
Accepted: 2 February 2024
Available online: 21 March 2024

KEYWORDS

Prechamber engines
Simulation investigation
Prechamber construction
Gas engines
Lean combustion

The research presented in this paper focused on the simulation analysis of the prechamber neck diameter on in-cylinder processes in a large gas engine. The investigation was conducted using AVL Boost software and the implemented PCSI combustion model. The scope of the analysis included different neck diameters from 17 to 26 mm and variations of the ignition timing in the range of 0 to 40 degrees. Using the narrowest ignition chamber neck resulted in the largest inter-chamber throttling effect. This translated into an increase in the maximum pressure in the cylinder, obtaining more heat release and the heat release rate. Further reduction of the constriction below 17 mm led to a rapid pressure increase in the ignition chamber at the start of combustion above the maximum pressure in the cylinder, for which the indicated constriction value was considered limiting.

1. Introduction

The world of rail transportation is continuously transforming, leading to a revolution in rail vehicle propulsion systems. From the days of steam locomotives to today's innovations, rail transportation propulsion technologies are changing, striving to increase performance, energy efficiency and reduce environmental impact [3]. The main trends in expanding powertrains, in addition to pure electric systems, focus on using alternative fuels or improving the energy characteristics of conventional drive trains.

Hydrogen as a fuel for rail transportation is being considered and implemented in terms of fuel cells or combustion in reciprocating engines [4, 10]. Subsequently, hybrid propulsion systems, often equipped with a CI engine and various energy recovery and storage systems, are being developed [6, 15]. An existing solution also powers powertrains with natural gas, stored in liquefied (LNG) or compressed (CNG) form [2, 7].

The fuelling of HD gas engines is carried out using a minimum ignition dose of diesel fuel for ignition or as spark-ignition engines. For spark-ignition engines, in order to increase the ignition energy, a divided combustion chamber is used by employing a prechamber (PC) as in the MAN E3872 or Wärtsilä 31SG engine [14, 16]. In this type of engine, the ignition of the charge in the cylinder occurs multi-point from jets of burning charge flowing out of the PC rather than from a spark, successively penetrating the combustion chamber in a radial way [11]. By this method, it is possible to extend the range of effective combustibility of the mixture beyond the $\lambda = 1.5$ value at which the conventional SI engine system becomes unstable [1, 13].

Engine performance and emissions are significantly affected by the geometry of the ignition chamber [9]. The authors of the study [12] investigated by simulation the effect of ignition chamber narrowing (3.3–5.3 mm), length of outflow nozzles (1–2 mm), and diameter of outflow holes (1.15–1.56 mm) using a model with a 2.1 dm^3 displacement, engine speed of

* Corresponding author: filip.szwajca@put.poznan.pl (F. Szwajca)

1200 rpm, and ignition timing of 15°CA bTDC. It was found that narrowing mainly affected pressure build-up and residence time, nozzle diameter on peak pressure, and residence time. The smallest effect was caused by changing the length of the outflow channels.

In a further study [15], the effect of reducing the PC volume by 20% and increasing it by 25% relative to the reference chamber was examined for stoichiometric and lean combustion from λ between 1.6 to 2.2. For the reference chamber, the highest efficiency was obtained at λ = 1.6, amounting to 36% sequentially for the smaller and larger chamber, a value of less than 35% at the same excess air ratio. The lowest THC emissions were obtained for the largest chamber, CO emissions were lowest for the smallest and largest chamber, and NO_x emissions were similar in each case analyzed.

In another approach, five ignition chamber geometries were experimentally tested with different hole locations and geometries with the same volume for four chambers and a smaller volume for chamber 5 [11]. The highest efficiency was obtained for the chamber with the smallest volume of 1.4 cm^3 and eight holes with a diameter of 1.15 placed radially. The lowest efficiency was obtained for the chamber with the highest number and diameter of holes.

Following the results of research on the ignition chamber geometry's influence on in-cylinder processes and engine performance, it was decided to evaluate the effects of isolating one variable: the chamber neck diameter. The purpose of the investigation is a simulation evaluation of the prechamber neck diameter effect on in-cylinder processes in terms of applications in a gas engine dedicated to rail vehicles.

2. Methodology

2.1. The model used for the analysis

The simulation investigation analyzed is dedicated to medium-speed HD engines applied in rail vehicles, stationary power generators, or marine vessels. The calculation was performed using AVL Boost software with a computational model (Fig. 1) covering one cylinder in the range of intake manifold – exhaust manifold, excluding other engine components. Components are designated by symbols such as E for engine, SB for system boundaries, MP for measuring point, and C for cylinder. The cylinder displacement is 5.8 dm^3, and brake mean effective pressure (BMEP) is estimated at 10 bar. The technical data of the C1 cylinder are presented in Table 1.

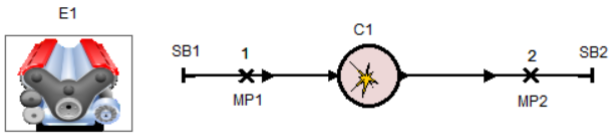

Fig. 1. View of the computational model

Table 1. Engine geometry specifications

Parameter	Unit	Value
Bore	mm	165
Stroke	mm	230
Compression ratio	–	12
Conrod length	mm	360
Piston bowl diameter	mm	100
Piston bowl depth	mm	20
Valve seat angle	deg	30

The object of the analysis is a methane two-stage combustion system therefore, a Calculated Heat Release Combustion Model called Pre-Chamber Spark Ignited Gas Engine (PCSI) was used for the calculations. It is a model where energy from the prechamber is used to initiate the combustion of the homogeneous mixture located in the cylinder. Such a system is used to burn a very lean mixture globally beyond the flammable limits using conventional spark ignition. A view of the analyzed prechamber, along with geometric features, is shown in Fig. 2. The ignition source is located at the top of the chamber, while the outflow nozzles are at the bottom.

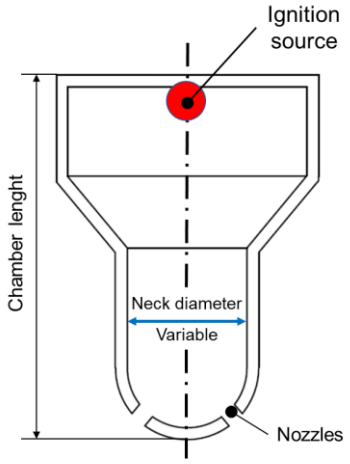

Fig. 2. Schematic of the pre-chamber used for the analysis, along with specific features

In order to achieve the work goal, four different diameters of the ignition chamber neck were selected in the range from 17 to 26, marked with the following symbols N1–N4, summarized in Table 2. The chamber's volume and length were the same for each case at 7.5 cm^3 and 5.5 cm, respectively. The configuration of the outflow channels included 8 holes with a diameter of 1.5 mm.

Table 2. Data set used for simulations – prechamber neck diameters

Label	Neck diameter [mm]
N1	17
N2	20
N3	23
N4	26

2.2. Simulation conditions

The simulation investigation was performed for a 1500 rpm engine speed at which a constant friction loss of 2 bar friction mean effective pressure (FMEP) was set. The cylinder has two valves, one intake and one exhaust, with 71 and 73 mm diameters, respectively. Employing species transport – classic for calculations, methane with an lower heating value LHV of 50 MJ/kg and an air demand of 17.2 was used as fuel. The fuel dose delivered to the cylinder and the ignition chamber was fixed at 300 and 3 mg, respectively. This yielded a mixture with an excess air ratio of $\lambda \sim 2.0$.

For the PCSI model, all turbulence coefficients were set to 1. According to the Petters et al. model [5, 8], the laminar flame correlation was used for combustion. The prechamber heat release rate coefficient and cylinder ignition ratio were set to 0.3 and 0.5, respectively, regardless of the operating point. The heat release rate coefficients for Phase 1 and Phase 2 were 1 and 1.5, respectively.

Turbulence and heat dissipation in the cylinder are calculated similarly to the combustion model of an open combustion chamber gas engine. The difference is an additional source of turbulence coming from the kinetic energy of the charge flowing through the flow channels described by the formula:

$$\frac{dk_{ori}}{dt} = C_{turb,ori} \cdot \frac{dm_{ori}}{dt} \cdot \frac{v_{ori}^2}{2} \frac{1}{m_{cyl}} \tag{1}$$

where $C_{turb,ori}$ to turbulence orifice constant, dm_{ori} is mass transfer, V_{ori} – is flow velocity and m_{cyl} is mass in the cylinder.

The initiation of the combustion process in the cylinder begins moments before the radius of the flame front R_f in the PC exceeds the length of the chamber l_{PC} according to the following equation:

$$\frac{R_f}{l_{PC}} > C_{ign} \tag{2}$$

The established initial conditions for the intake and exhaust systems, as well as the cylinder at the time of exhaust opening (EO), are summarized in Table 3 below.

A modified "Woschni 1978 Zapf" heat transfer model [18, 19] was adopted for the calculations. The thermodynamic conditions used are shown in Table 4.

Table 3. Initial conditions used for simulation

Intake duct		
Parameter	Unit	Value
Pressure	bar	3.00
Temperature	K	340
Gas	–	Air
Cylinder – exhaust open		
Pressure	bar	7
Temperature	K	820
A/F ratio	–	33.5
Exhaust duct		
Pressure	bar	2.7
Temperature	K	500
Gas	–	Combustion products

Table 4. Heat transfer area and thermal input data

Piston		
Parameter	Unit	Value
Surface area	cm^2	236
Wall temperature	K	250
Cylinder head		
Surface area	cm^2	221
Wall temperature	K	250
Liner		
Surface area (TDC)	cm^2	10
Wall temperature (TDC)	K	200
Wall temperature (BDC)	K	150

2.3. Results processing

The simulation framework included calculations for 36 engine operating points. Four dimensions of the ignition chamber neck and nine values of the ignition advance angle in the range from 0 to 40 degrees before TDC in increments of 5 degrees were analyzed. The results obtained were Traces as a function of crankshaft angle (0.1 deg accuracy) and transient, which means cycles (9 consecutive cycles were simulated).

The pressure differences between the cylinder and the ignition chamber were determined by the formula:

$$\text{Diff MC\_PC} = P_{MC} - P_{PC} \tag{3}$$

where P_{MC} is cylinder pressure, P_{PC} is prechamber pressure.

The cubic spline interpolation method implemented in AVL Concerto software was used to make contour maps. The combustion time was calculated based on the values of the angle for which 10 and 90% of the charge was burned according to the formula:

$$\text{CA90\_CA10} = \text{MBF90} - \text{MBF10} \tag{4}$$

The amount of accumulated heat was calculated based on the heat release rate (HRR) relative to the crankshaft angle α according to the formula:

$$Q = \int_{SOC}^{EOC} \frac{HRR}{d\alpha} d\alpha \tag{5}$$

The other indicators of the combustion process included in the article are directly derived from the simulations carried out, requiring no further calculation.

3. Results

3.1. Effect of neck diameter on cylinder pressure

The maximum cylinder pressure marked as Pcyl_max obtained for the studied engine operation field (four neck diameters, nine ignition points) is shown on the contour map (Fig. 3). The color scale starts from blue for the smallest value to red for the largest. The black points indicate the points at which the simulation was directly carried out.

Decreasing prechamber neck diameter results in obtaining higher and higher maximum pressure for a constant value of the ignition advance angle. The same tendency was obtained for increasing ignition timing advance. Comparing the two combustion control parameters, the ignition timing relative to the PC narrowing has a much greater effect on peak pressure. For a chamber with a 20 mm neck and ignition at TDC, the maximum pressure is 56.29 bar, while an ignition timing advance of 30 degrees increases peak pressure to 130.06 bar. In comparison, the difference in peak pressure for 20 deg ignition timing advance between chamber N1 and N4 is 4.78 bar.

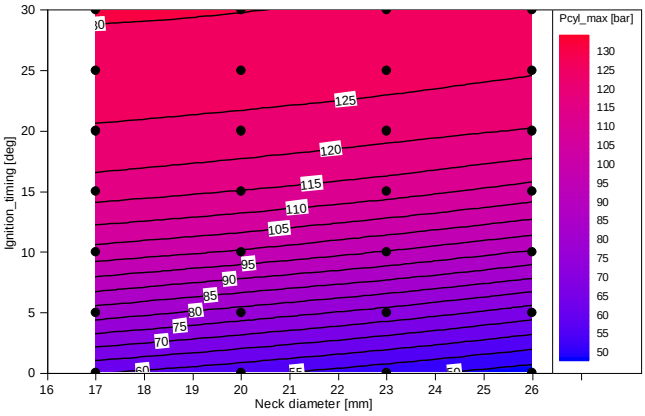

Fig. 3. Contour map of maximum cylinder pressure

In the next map, the value of the maximum pressure and its position relative to the crank angle marked as APmax was determined (Fig. 4). The values shown in the map indicate the position of Pcyl_max after TDC. The position of Pcyl_max significantly affects engine performance. However, suppose Pcyl_max is in the very close area of TDC or before TDC. In that case, it significantly increases mechanical losses and, under actual operating conditions, leads to damage in the engine's crank-piston system. In the analyzed conditions, an ignition advance of more than 30 degrees results in the transfer of Pcyl_max before TDC; therefore, 30 degrees was considered the limit of the simulation. This limit is marked with a bold line on the map.

Reducing the prechamber flow neck diameter shortens the time between ignition and reaching maximum pressure. The change in the position of APmax parameter is most evident for the smallest ignition advance sequentially. The intensity of change decreases with increasing ignition advance. For an N2 chamber characterized by a 20 mm diameter narrowing, APmax ranges from 23.3°aTDC for 0°CA ignition timing to 0.4°bTDC for 35°CA ignition timing. The largest ignition advance angle analyzed for the N2 chamber at which APmax is after TDC is 25°CA. Increasing the diameter of the ignition chamber neck delays the initiation of the main charge combustion process, which allows the use of larger ignition advance angle values.

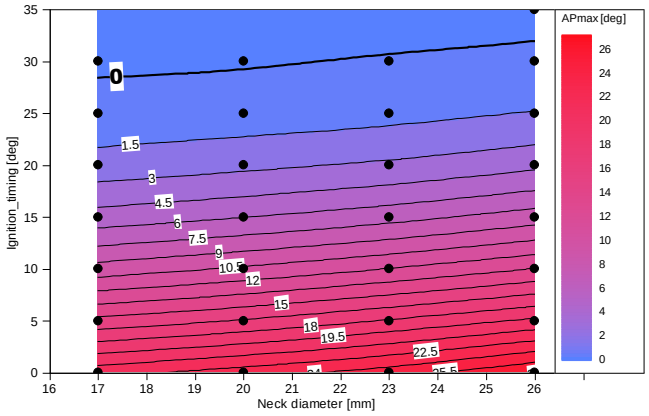

Fig. 4. Contour map of maximum cylinder pressure position relative to TDC

An indicator graph for the N2 chamber and four successive values of the ignition advance angle starting at 10°CA bTDC is shown in Fig. 5. The red color indicates the pressure in the cylinder, the blue color in the ignition chamber, while the black dotted line indicates the pressure difference. The value of MC_PC_diff below zero indicates the flow of charge from the ignition chamber to the cylinder, above the flow from the cylinder to the chamber.

A specific feature of two-stage combustion is the rapid pressure increase in the prechamber, visible on the indicator diagram, and the pressure differential caused by inter-chamber throttling through the outflow channels.

The gradual advance of ignition causes a reduction in maximum pressure during the ignition event, and the waveform is much smoother. This is due to a faster build-up of pressure in the cylinder, which translates into a damping effect of back pressure. The MC_PC_diff curve illustrates this, the minimum of which becomes smaller and smaller with increasing ignition advance.

An ignition advance of less than 10°CA bTDC recorded a significantly higher PC pressure than MC

pressure at the ignition event. It means that the analyzed ignition chamber model with characteristic coefficients causes too much flow throttling. In contrast, for an ignition advance higher than 25°CA bTDC, the occurrence of Pmax before TDC was recorded. Both of these aspects are very unfavorable for the actual system configuration.

Regardless of the ignition advance analyzed, every single time, the maximum pressure in the prechamber occurs later than in the cylinder. This is also the result of inter-chamber throttling.

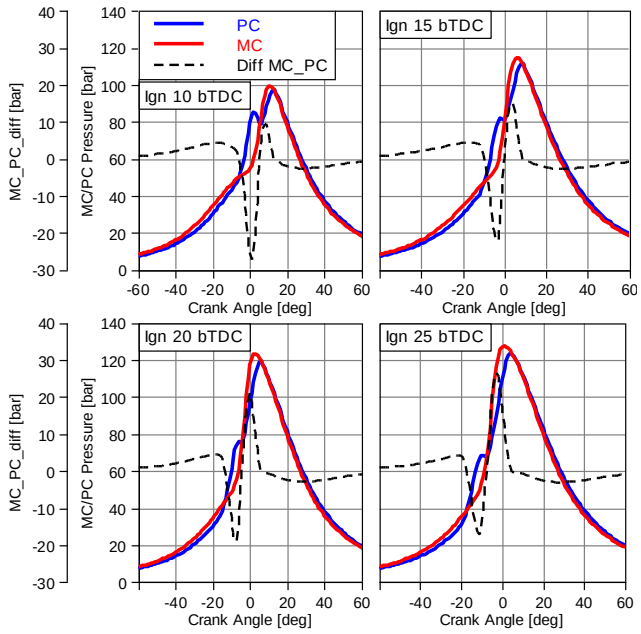

Fig. 5. Indicator diagrams for subsequent ignition advance values

The effect of the PC throttling size on the indicator diagram is shown in Fig. 6 at a constant ignition advance of 15°CA bTDC. The largest narrowing generates the largest pressure difference during the ignition event, particularly between the N1 and N2 chambers (black dashed line). The reduced pressure differential during the ignition event is also accompanied by a lower pressure differential when combustion starts in the cylinder. Relative to adjusting the ignition advance, different neck diameters generate smaller differences in the indicator graph.

An analysis of the maximum pressure rise rate as a function of ignition timing is shown in Fig. 7. The largest differences in the effect of using various prechamber models were observed in the range of ignition timing from 5 to 20°CA. The smallest, however, is for 30°CA and 0°CA, where model tests deviate significantly from the values obtained during experimental testing. Increasing the narrowing significantly increases the rapidity of pressure rise during ignition of the charge in the cylinder, which correlates to inter-chamber throttling.

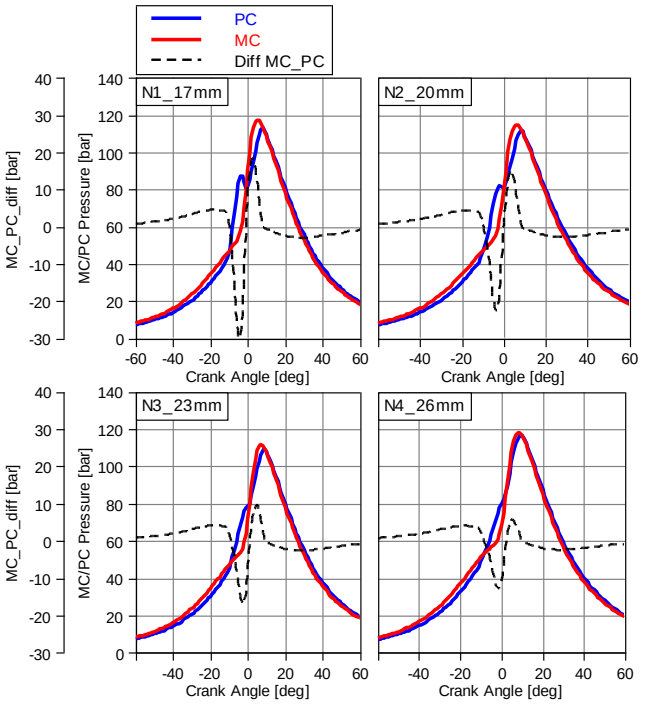

Fig. 6. Indicator diagrams for subsequent prechamber neck diameter

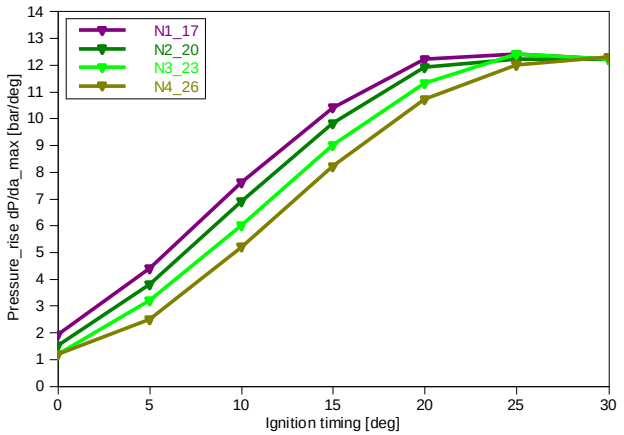

Fig. 7. Diagram of cylinder pressure rise rate for different prechamber neck diameters

3.2. Charge flow between the main and pre-combustion chambers

When analyzing the results of experimental studies, mass transfer between chambers is most often represented as a pressure difference. For the mentioned studies, the problem with determining the mass of the charge flowing between chambers is due to the impossibility of determining the charge's temperature. When using 0D simulations with the PCSI model, it is possible to represent the mass that flows between chambers during the operating cycle more accurately.

For the investigated engine operating points, the maximum pressure difference between the cylinder and the ignition chamber was calculated (Fig. 8). Due to the mode of the two-stage system, regardless of the

operating point, the largest pressure difference occurs during the ignition event. The increase in the mentioned difference for decreasing the ignition timing is mainly due to reducing the cylinder pressure relative to the ignition chamber and keeping the model settings constant regardless of the operating point. The largest pressure difference was recorded for the N1 chamber at which the charge is ignited from the spark plug and has the smallest cross-sectional distance to travel.

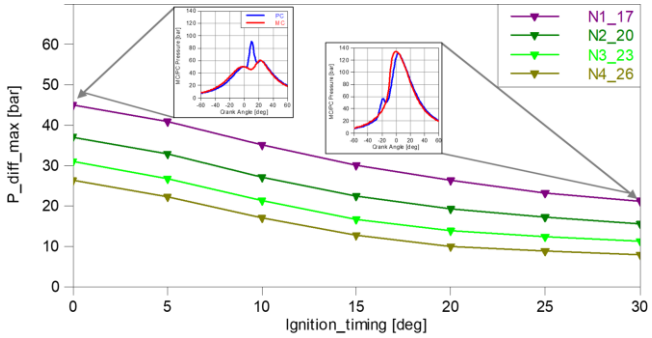

Fig. 8. Maximum pressure difference existing between the cylinder and the prechamber

Utilizing the advantage of 0D modeling in the form of identifying mass transfer between chambers is shown in Fig. 9. Values below zero indicate flow to the PC above, from the PC to the cylinder. Assuming a constant ignition chamber volume, the largest values of a mass flow rate of the charge at the ignition event were recorded for chamber N1. This further results in the highest flow at the ignition event of charge in the cylinder and backflow to the ignition chamber.

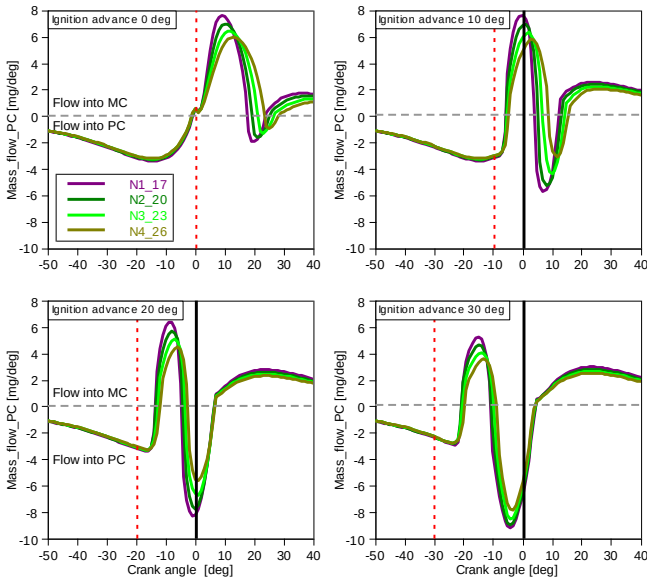

Fig. 9. Mass transfer between chambers for variable ignition advance

The nature of the changes depends on the ignition advance. For ignition at TDC, a slight break is visible due to the movement of the piston towards the bottom dead center, which is not visible for the other ignition timing values. As ignition advance decreases, the flow rate from the PC to the cylinder decreases, and an increasing flow rate from the cylinder to the PC is achieved at the start of combustion, which is related to the rate of pressure build-up.

3.3. Heat release calculation

The characteristics of the heat release rate (Fig. 10) are the same as those of the pressure rise rate presented previously. The additional turbulence energy introduced by the inter-chamber motion increases the intensity of the processes taking place in the cylinder. For ignition timing values in the range of 0°CA to 20°CA, the largest is obtained for chamber N1. The tendency changes at an ignition advance of 25°CA where dQmax begins to decrease, and the same results were obtained for chambers N1 and N3.

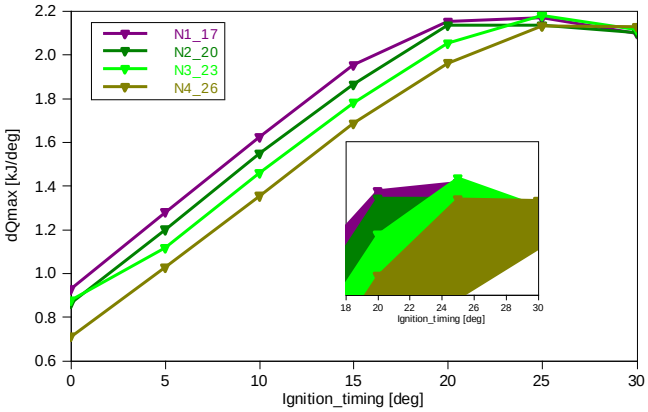

Fig. 10. Heat release rate graph versus ignition timing

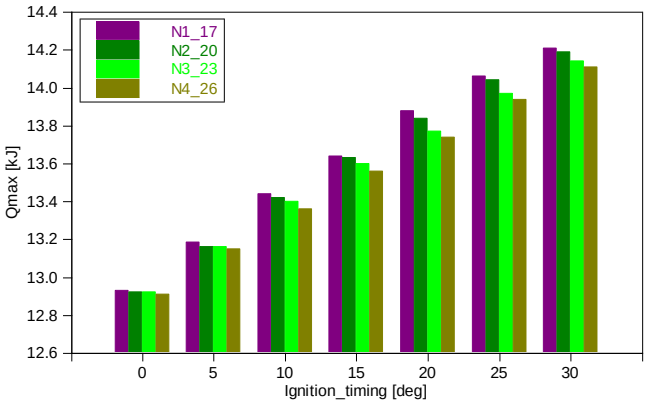

Fig. 11. Diagram describing the amount of accumulated heat

The accumulated heat (Fig. 11) was determined from dQmax that the obtained character of the curve is the same. The smallest predominance of the accumulated heat amount when analyzing chamber N1

occurs for 15°CA ignition timing, while the largest occurs for 20°CA. For ignition timing values of 5°CA, the results of chambers N2 and N3 are very similar. At the same time, it should be noted that for each point analyzed, the energy supplied in fuel was 15.15 kJ.

3.4. Evaluation of combustion phases

The combustion analysis is presented as combustion duration between an angle of 10% and 90% of the heat released (CA90_CA10) and the angle at which 10% of the charge was burned (Fig. 12). The ignition advance angle most influences CA10, as it increases, the effect of inter-chamber throttling was noted to decrease. Increasing the effect of inter-chamber throttling accelerates the penetration of the ignition charge in the cylinder and the ignition of a lean homogeneous mixture. It translates directly into combustion time, which decreases with the selection of increasingly favorable ignition timing.

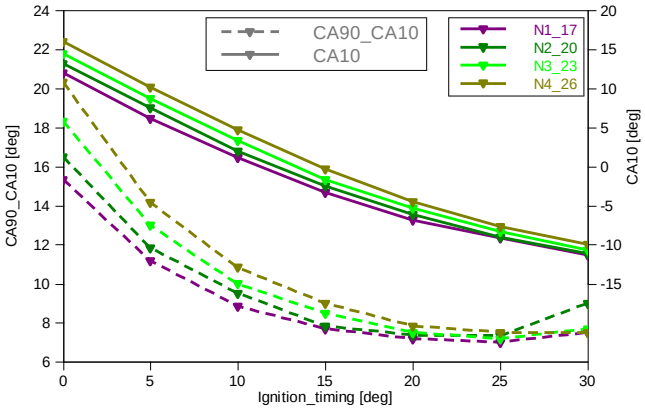

Fig. 12. Diagram representing combustion time and CA10 values

4. Conclusions

Conducting 0D simulations with the implemented PCSI calculated heat release model for a gas engine allows determining a series of parameters characterizing the SI engine operation with a prechamber of the so-called two-stage combustion system. The effect of the prechamber neck diameter on the thermodynamic parameters of the combustion process was analyzed with the model coefficients fixed.

It has been shown that a reduction in neck diameter in the range of 26–17 mm results in increased turbulence powered by the kinetic energy of inter-chamber throttling. This translates into increased combustion rates and improved performance in the analyzed range of ignition advance angle for a constant crankshaft speed and fuel consumption value.

For a chamber with a 20 mm neck and ignition at TDC, the maximum pressure is 56.29 bar, while an ignition timing advance of 30 degrees increases peak pressure to 130.06 bar. In comparison, the difference in peak pressure for 20 deg ignition timing advance between chamber N1 and N4 is 4.78 bar. For an N2 chamber characterized by a 20-mm diameter narrowing, APmax ranges from 23.3°aTDC for 0°CA ignition timing to 0.4°bTDC for 35°CA ignition timing. This correlation shows a higher sensitivity of the change in thermodynamic indicators relative to the ignition advance than the change in the neck diameter of the pre-combustion chamber.

With a fixed set of model coefficients, no combustion deterioration phenomena were associated with incorrect setting parameters or system geometry as occurs in real engines. This prompts further simulation analysis with support of experimental results.

Acknowledgements

This work has been done under AVL University Partnership Program and support by Subvention of Polish Ministry of Higher Education, project 0415/SBAD/0343.

Nomenclature

BMEP	brake mean effective pressure
CA	crank angle
CI	compression ignition
CNG	compressed natural gas
CO	carbon monoxide
DI	direct injection
FMEP	friction mean effective pressure
HD	heavy duty
LHV	lower heating value
LNG	liquefied natural gas
LPG	liquefied petroleum gas
MC	main chamber
NO_x	nitrogen oxides
PC	prechamber
PCSI	prechamber spark ignited
SI	spark ignition
TDC	top dead centre
THC	total hydrocarbon
λ	air-fuel equivalence ratio

Bibliography

[1] Bunce M, Blaxill H. Methodology for combustion analysis of a spark ignition engine incorporating a pre-chamber combustor. SAE Technical Paper 2014-01-2603. 2014. https://doi.org/10.4271/2014-01-2603

[2] Freightwaves.com. https://www.freightwaves.com/news/is-compressed-natural-gas-finally-feasible-for-railroad-applications (accessed on 2023.12.03).

[3] Dincer I, Hogerwaard J, Zamfirescu C. Clean rail transportation options. Springer Cham. 2016. https://doi.org/10.1007/978-3-319-21726-0

[4] Gallas D, Stobnicki P, Bolzhelarskyi Y. Types and applications of hydrogen fuel cells in transport. Rail Vehicles/ Pojazdy Szynowe. 2022;3-4:31-36. https://doi.org/10.53502/RAIL-157018

[5] Goettgens J, Mauss F, Peters N. Analytic approximation of burning velocities and flame thickness of lean hydrogen, methane, ethylene, ethane, acetylene and propane flames. 24th Symposium (International) on Combustion. The Combustion Institute. Pittsburgh 1992.

[6] Kurc B, Woźniak K, Rymaniak Ł, Szymlet N. Integration of capacitors with carbon-lignin based electrodes in rail vehicles for enhanced energy efficiency. Rail Vehicles/Pojazdy Szynowe. 2023;3-4:33-39. https://doi.org/10.53502/RAIL-176155

[7] Lipskis I, Pukalskas S, Droździel P, Barta D, Žuraulis V, Pečeliūnas R. Modelling and simulation of the performance and combustion characteristics of a locomotive diesel engine operating on a diesel–LNG mixture. Energies. 2021;14(17): 5318. https://doi.org/10.3390/en14175318

[8] Mueller UC, Bollig M, Peters N. Approximations for burning velocities and Markstein numbers for lean hydrocarbon and methanol flames. Comb Flame. 1997;108:349-356. https://doi.org/10.1016/S0010-2180(96)00110-1

[9] Pielecha I, Bueschke W, Skowron M, Fiedkiewicz Ł, Szwajca F, Cieślik W et al. Prechamber optimal selection for a two stage turbulent jet ignition type combustion system in CNG-fuelled engine. Combustion Engines. 2019;176(1): 16-26. https://doi.org/10.19206/ce-2019-103

[10] Pielecha I, Engelmann D, Czerwinski J, Merkisz J. Use of hydrogen fuel in drive systems of rail vehicles. Rail Vehicles/Pojazdy Szynowe. 2022;1-2:10-19. https://doi.org/10.53502/rail-147725

[11] Shen F, Totsuka M, Kuboyama T, Moriyoshi Y, Yamada T, Shimizu K et al. Effects of pre-chamber specifications on lean burn operation in a pre-chamber engine with fuel reformed gas. SAE Technical Paper 2023-32-0007. 2023. https://doi.org/10.4271/2023-32-0007

[12] Silva M, Sanal S, Hlaing P, Cenker E, Johansson B, Im HG. Effects of geometry on passive pre-chamber combustion characteristics. SAE Technical Paper 2020-01-0821. 2020. https://doi.org/10.4271/2020-01-0821

[13] Stadler A, Wessoly M, Blochum S, Härtl M, Wachtmeister G. Gasoline fueled pre-chamber ignition system for a light-duty passenger car engine with extended lean limit. SAE Int J Engines. 2019;12(3):323-339. https://doi.org/10.4271/03-12-03-0022

[14] Truck MAN, Bus SE. MAN E3872 gas engine. https://www.man.eu/engines/en/products/power-generation/gas/man-motor-e3872.html (accessed on 2023.1.03).

[15] Ugrinić S, Dilber V, Sjeric M, Kozarac D, Krajnovic J, Tomic R. Experimental study of pre-chamber geometry influence on performance and emissions in a gasoline spark ignited engine. SAE Technical Paper 2022-01-1008. 2022. https://doi.org/10.4271/2022-01-1008

[16] Urbański P, Gallas D, Stachowicz A, Jakuszko W, Stobnicki P. Analysis of the selection of the auxiliary drive system for a special purpose hybrid rail vehicle. Rail Vehicles/Pojazdy Szynowe. 2022;1-2:30-39. https://doi.org/10.53502/rail-149405

[17] Wärtsilä Corporation. Product Guide, Wartsila 31SG, September 2019.

[18] Woschni G. A universally applicable equation for the instantaneous heat transfer coefficient in internal combustion engines. SAE Technical Paper 67009319. 1967. https://doi.org/10.4271/670931

[19] Zapf M. Beitrag zur Untersuchung desWaermeuebergangs Waehrend des Ladungswechsels ineinem Viertakt-Dieselmotor. Motortechnische Zeitschrift. 1969;30(12):461-465.